

**Analyzing the Fine Structure of Hg<sup>198</sup>  
Through the Zeeman Effect**

**Completed for Certificate in Scientific  
Computation**

Martin A Valenzuela

Faculty Research Advisor

---

Greg O. Sitz PhD

SSC-479R Summer 2014

# 1 Executive Summary

Quantum mechanical processes are often difficult to observe due to their intrinsic small scale. However, the observation of these processes can yield benefits in macro scale applications such as carbon dating, communications, spectroscopy, and others. One such quantum mechanical processes is the Zeeman effect. The Zeeman Effect provides a method to observe the change in quantum mechanical energy levels due to the presence of an external magnetic field. With the advent of high resolution interferometry, a classical spectrometer is no longer needed to perform this observation. [1]

Spectral interferometry recorded by digital photography provides a method to analyze the visual data in an automated manner. The analysis of spatially resolved imaging using a scripting language such as python provides the automated method. We examine the Zeeman Effect of  $\text{Hg}^{198}$  discharge lamp within a magnetic field range of  $.47 \pm .008$  Tesla to  $.83 \pm .008$  Tesla. With the use of python, fluctuations in the intensities of the rings visible through an interferometer can be averaged out and provide a greater confidence in the observed values.

The examination of the behavior of the  $6s7s\ ^3S_1\ m_j=-1$  to  $6s6p\ ^3P_2\ m_j=-1$  spin state transition of a  $\text{Hg}^{198}$  discharge lamp in the magnetic field, produced a linear relation for the change in spatial frequency and magnetic field of  $-23.74 \pm 4.17\ \text{mm}^{-1}\text{T}^{-1}$  with an intercept of  $.83 \pm 2.76\ \text{mm}^{-1}$ . Similarly, a linear relationship of  $28.11 \pm 3.09\ \text{mm}^{-1}\text{T}^{-1}$  with an intercept of  $-4.50 \pm 2.05\ \text{mm}^{-1}$  was found for the  $6s7s\ ^3S_1\ m_j=1$  to  $6s6p\ ^3P_2\ m_j=1$  spin state transition. The linear values differ from the accepted values by +2% and +20% respectively. The accepted values are  $-23.33\ \text{mm}^{-1}\text{T}^{-1}$  for the  $m_j=-1$  transition and  $23.33\ \text{mm}^{-1}\text{T}^{-1}$  for the  $m_j=1$  transition. Using the implemented method to analyze the  $m_j=-1$  state transitions provides a moderately agreeable result, however, in future investigations, a different method must be employed to calculate the  $m_j=1$  state transitions that account for the susceptibility of the method to off axis intensity peak skewing.

## 2 Introduction

### 2.1 Physics Motivation

The magnetic field induced splitting of spin orbital coupled states in  $\text{Hg}^{198}$  atoms can account for the change in interference patterns of light produced by a  $\text{Hg}^{198}$  lamp. The quantum numbers for the spin angular component and for the orbital angular component must be combined in order to remove degeneracies and conserve angular momentum. However, the spin component also has magnetic properties which when stimulated by a magnetic field, can break the coupling and degeneracy in to distinct states which can create observable bands of energy. This use of a magnetic field is the Zeeman Effect and demonstrates the quantization of angular momentum in quantum structures. [7]

### 2.2 Theoretical background

#### 2.2.1 Photon Emission

The  $\text{Hg}^{198}$  lamp produces light through photon emission. The  $\text{Hg}^{198}$  atoms absorb the energy provided by a power supply through excitation of its valence electrons. The excited electrons drop from their excited  $6s7s\ ^3S_1$  state to the  $6s6p\ ^3P_2$  and emit photons with wavelength of 546.07 nm. [2] These emitted photons are in the visible light range and so can be documented with conventional photography. [6] A more detailed look at the Hg states is provided in Appendix A.

#### 2.2.2 Perturbation Theory

The structure of the  $\text{Hg}^{198}$  is altered when a uniform magnetic field  $B$  is present. In order to treat these conditions it is necessary to treat the issue with Perturbation Theory. The correct Hamiltonian is made of the typical Hamiltonian with an added spin orbital correction, and a magnetic Field term. [7] The Hamiltonian produces a degeneracy which is lifted by an external magnetic field.

The degeneracy for the  $6s6p\ ^3P_2$  state is resolved by splitting in to 5  $m_j$  states; -2, -1, 0, 1, 2. Likewise, the degeneracy for the  $6s7s\ ^3S_1$  state is resolved to 3  $m_j$  states. [5] Of the split state transitions from  $6s7s\ ^3S_1$  to  $6s6p\ ^3P_2$ , three transitions emit a plane polarized photon. This is shown in Figure 1. These  $\Delta m_j=0$  state transitions were of primary focus to examine the Zeeman Effect. When an external magnetic field is present, the change in energy levels are given by equation 1.

$$\Delta E = g_F \mu_B m_j B \quad (1)$$

$\Delta E$  is the change in energy from the original un-split state transition;  $g_F$  is the combined g-factor that results from the vector combination discussed in appendix D for equation 4;  $\mu_B$  is the Bohr magneton;  $m_j$  is the  $\hat{Z}$  projection of the spin-orbit coupled vector  $\vec{F}$  (See appendix D);  $B$  is the magnetic field. [7] The theoretical values are provided in Appendix B in Figure 9.

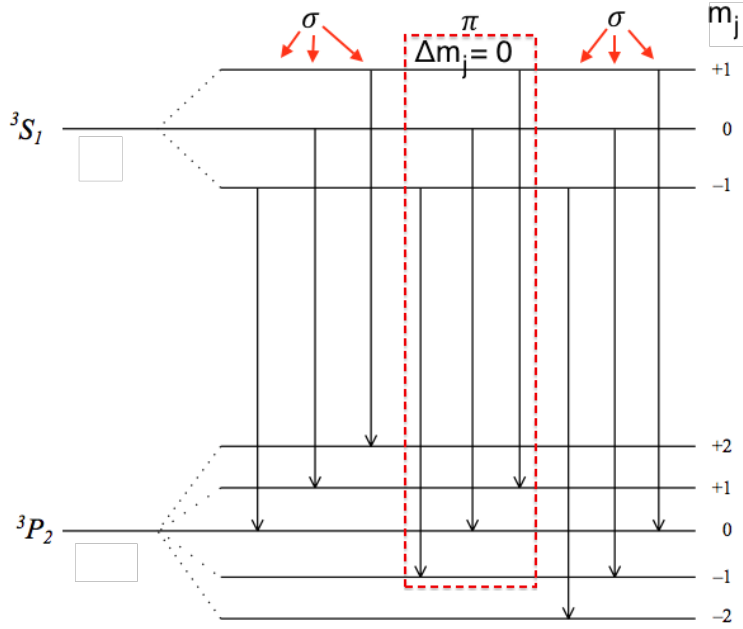


Figure 1: Depicted are the split states of  $6s7s\ ^3S_1$  with arrows connecting to the possible transition states of  $6s6p\ ^3P_2$  when the external magnetic field  $B \neq 0$ .  $\sigma$  and  $\pi$  describe the effective polarization of the emitted photon for the specific transition. Transitions that are  $\Delta m_j \neq 0$  are of  $\sigma$  polarization and were filtered out by the polarizer.

It is this change in photo emission energy we are investigating by using a variable magnetic field.

### 2.2.3 Fabry-Perot Etalon Optics

The Fabry-Perot etalon is made of two parallel reflective pieces of glass. These pieces of glass come in variable reflective grades so as to control the amount of light which passes through each. As the light passes through glass A, a portion of the light is reflected. The part of the light that is not reflected passes through glass A into the space between glass A and glass B. A part of the light will then become reflected between glass A and glass B and another part will transmit through the glass. Due to the light being reflected between the two pieces of glass this process will happen recursively as illustrated in Figure 2. This recursive reflection a pattern of coherence and interference in the form of bright rings separated by dark bands as seen in Figure 3. The reflectivity of the two pieces of glass will determine the sharpness of the ring intensity peaks. This quality in the reflectivity is also referred to as finesse. [6]

The ring pattern changes as a magnetic field is provided to the lamp source. Each bright ring will split according to the model developed in Figure 1. The relative radii of the rings provide the change in spatial frequency for the  $m_j = -1$  and the  $m_j = +1$  transition from the  $m_j = 0$  transition through the



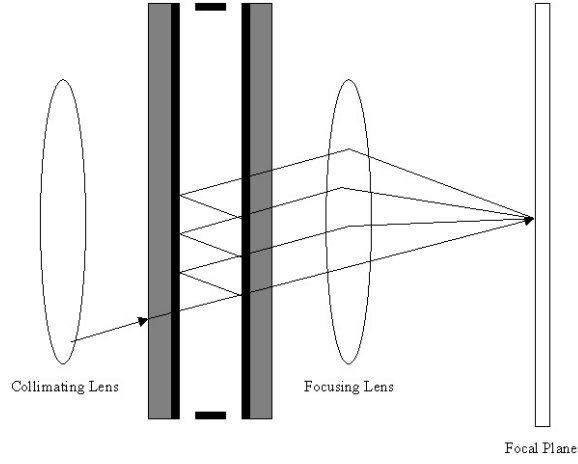


Figure 2: Light propagation through a Fabry-Perot etalon.

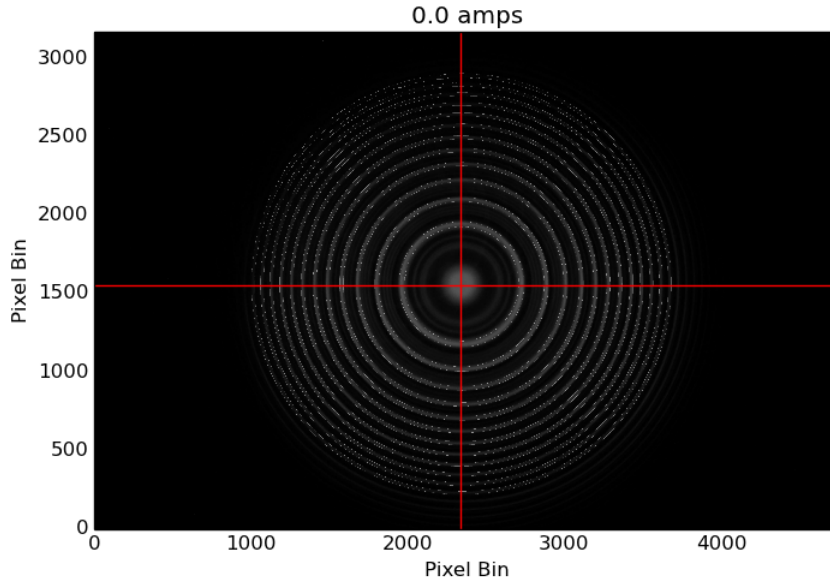


Figure 3: Fringe pattern of  $\text{Hg}^{198}$  with no magnetic field . This fringe pattern is used to provide a guide line to find the radii for the images involving a non-zero magnetic field.

use of the following equation

$$\Delta\nu = \frac{1}{2d} \left( \frac{R_{m_j=\pm 1}^2 - R_n^2}{R_n^2 - R_{n+1}^2} \right) \quad (2)$$

$R_n$  is the radius, in pixels, of the nth ring.  $R_{n+1}$  is the radius, in pixels, of the

nth + 1 ring.  $R_{m_j=+1}$  corresponds to the radius, in pixels, to the  $m_j = +1$  ring of the nth ring. Like wise  $R_{m_j=-1}$  is the radius to the  $m_j = -1$  ring of the nth ring.

### 2.3 Our approach

The observation of the splitting of Hg atom states is difficult due to narrow differences in the wavelength of the emitted photons to resolve. [6] Use of a Fabry-Perot etalon provides greater detail of the spectrum as we vary the magnetic field. Small differences in the wavelength are visible through the photography of the interference pattern, as in Figure 3. Once photographed, we determine the relation between the radii of the rings created by the interference pattern of the Hg light, and use Equation 2 to calculate the change in spatial frequency of the splitting of the  $^3S_1$ - $^3P_2$  transition by the magnetic field.

## 3 Experimental setup

### 3.1 Apparatus

The setup is shown schematically in Figure 4 and consists of a Hg<sup>198</sup> Lamp which is placed within an electromagnet. The lamp is powered by a 1500V AC power supply. The power supply for the electromagnet provided as DC and has a range of 0-10amps. This range provides a magnetic field up to approximately .808 Tesla. The magnetic field was measured using a F. W. Bell 4048 Tesla meter. The current and therefore the magnetic field are the only elements of the experiment that were varied.

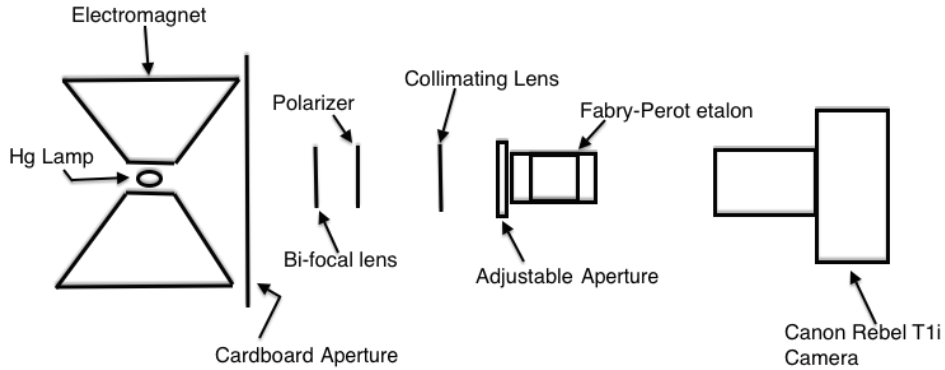


Figure 4: Apparatus layout as seen from the top. Not to scale.

Limiting the amount of light visible from the lamp was a sheet of cardboard with a two inch in diameter opening. The light from the lamp would pass through the opening and arrive at the focusing lens. Between the focusing lens and its focal point the light will travel through a polarizing screen to filter out the  $\sigma$  transitions. The light is focused at .5 cm from the collimating

lens. Once the light is collimated it passes through an aperture which regulates the light entering the Fabry-Perot etalon, thereby reducing glare from the walls of the etalon. The reflective lenses in the etalon are separated by 10mm. Using a Canon T1i Camera equipped with a EF55-250mm lens we were able to magnify and capture the interference pattern. The camera settings are shown in Table 1. Unlike previous efforts there was no color filter used as part of the equipment. By not using a physical color filter the image captured greater intensity values. Color filtering was done digitally and is further discussed in section 4.1.1.

| Focal Ratio | ISO | Exposure Time | Focal Length |
|-------------|-----|---------------|--------------|
| 5.6         | 400 | 2 second      | 240 mm       |

Table 1: Canon Rebel T1i DSLR camera settings used for image capture.

## 3.2 Data Collection

### 3.2.1 Magnetic Field Calibration

The current powering the electromagnet was the variable in the experiment. Because of its adjustment throughout the experiment we calibrated the electromagnet using the F. W. Bell 4048 Tesla meter. First we took readings of the magnetic field without the Hg tube at the center of the electromagnet. We affixed the sensor so that it would lie in the position the Hg lamp would be within the electromagnet. The electromagnet was then turned on and the amperage was varied at different increments.

Column 2 in Table 2 shows the recorded reading of the magnetic field. Due to possible loss in fidelity from heat we repeated the same procedure after the magnet was in use for over 20 minutes. This amount of change will result in a slight error for the data taken as time progresses and so we have propagated the error through to the measurement of the frequencies of light by considering an increase in uncertainty as each measurement is taken. The measurements of the magnetic field were recorded prior to taking the photography in order to find a relation between the current provided to the electromagnet and the strength of the magnet without having to remove the Hg lamp at each step of taking data and thereby minimizing systematic error. Figure 5 shows the near linear relation between the current and magnetic field strength.

| Current | Magnetic Field $\pm .008$ (Tesla) |
|---------|-----------------------------------|
| 3       | .465                              |
| 3.4     | .53                               |
| 3.8     | .59                               |
| 4.2     | .651                              |
| 4.6     | .712                              |
| 5.0     | .774                              |
| 5.4     | .832                              |

Table 2: Varied current supplied to electromagnet with corresponding magnetic field readings using the F. W. Bell 4048 Tesla meter.

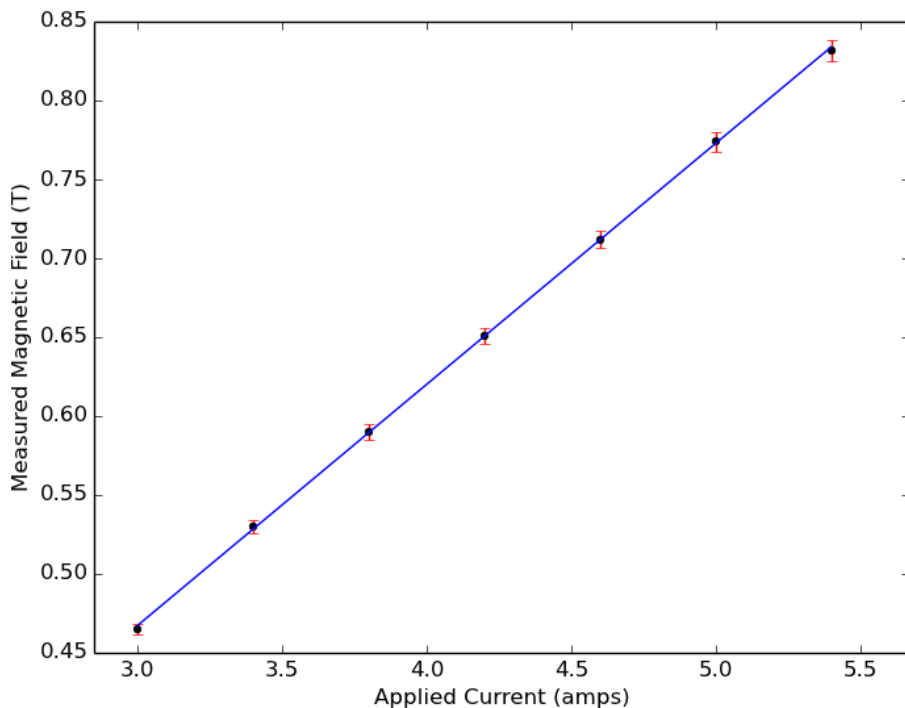


Figure 5: Plot of Table 2 with fit lines. The numbers correspond to the points for that particular recording of magnetic field. The error bars displayed account for the uncertainty in the electronics in the power supply, and the F. W. Bell 4048 Tesla meter. Also the error bars take in to account variability in static observed magnetic reading of  $\pm .008$  Tesla. Lastly, they also account for an increase in uncertainty as the amps are increased due to better fit lines of a quadratic nature. [13]

## 4 Data Analysis and Results

### 4.1 Data Processing and Hypothesis Testing

The photography of the interference patterns for each amperage setting look similar to Figure 3 except with changes to the number of the rings visible. Full sets of images are available in Appendix C. The images taken, however, also exhibit fringes from photon emission of transitions to the  $6s6p\ ^3P_0$

(violet), and  ${}^3P_1$ (blue) states. See Figure 8. [3] As part of this experiment we only focused on the transition of the  ${}^3S_1$  to  ${}^3P_2$  where  $\Delta m_j=0$ , and thus filtered out any non-green elements through the use of the python scripting language. More detail on the filtering is provided in Appendix E.1. Once the image data was reduced to the green light data, the data was run through a program written in python for this experiment. [8]

#### 4.1.1 Python Script Methodology

Using the python scripting languages, the images were processed before any data was extracted. The images were first reduced to their green components eliminating the contributions of other state transitions present within the Hg lamp. See Appendix E.1. Next, the Canny method, part of the Scikit-Image processing package, [9] was used on the image as a means to detect the edges of the fringes in the zero Tesla image. This image, being the image with the most pronounced intensity peaks, provided a means to calibrate all other images taken while a magnetic field was present. See Figure 6 for further description. The zero magnetic field image provided boundaries to search for the  $m_j=0$  light emission of the  ${}^3P_2$  transition for each of the non-zero magnetic field images.

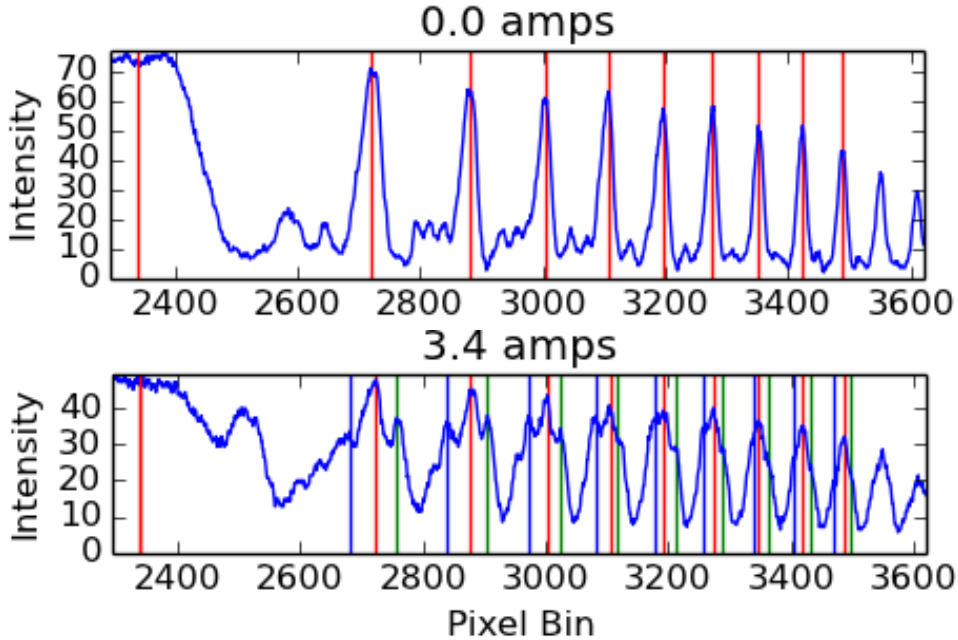


Figure 6: The plots display the intensities for the right half of the center cross section. Green lines are the locations for the  $m_j=-1$  transition intensity peaks, and blue lines are for the  $m_j=1$  transitions. The red line near the left edge in the plots, is the center of the rings along the x axis and each following red line are the locations of the  $m_j=0$  transition intensity peaks. See Appendix E.2 for further description

In Figure 13 the Canny function defines intervals in which primary intensity

peaks can be found. These intervals along with the found intensity peaks for the zero magnetic field image are carried through and used to determine the location of the primary peak ( $m_j=0$ ), the  $m_j=-1$ , and  $m_j=1$  intensity peaks along the entire vertical and horizontal cross-sections of each image taken at a nonzero magnetic field, such as in Figure 12. In order to determine the radii of each fringe, the hough circle method was used to estimate the center of the fringes to trace out the detected edges by the Canny function. This method is further discussed in Appendix E.3

Once the center is detected the radii of each peak was calculated and this allowed the calculation of the spatial frequency given two sequential peaks. However, due to the multiple ring pattern in the images, multiple spatial frequency values could be calculated, approximately 24 values for the horizontal cross-section and 17 values for the vertical cross-section for  $m_j=-1$  and also for  $m_j=1$ . The calculations were done in this manner for each of the images taken at the corresponding magnetic field listed in Table 2. The multiple values were averaged and provided a confidence level in the measurement.

| Amps | Calculated Magnetic Field $\pm .008$ (Tesla) | $\Delta\nu$<br>$m_j=+1$ ( $\text{mm}^{-1}$ ) | $\Delta\nu$<br>$m_j=-1$ ( $\text{mm}^{-1}$ ) |
|------|--|--|--|
| 3    | .467   | $9.87 \pm .87$                               | $-8.72 \pm 1.03$                             |
| 3.4  | .528   | $10.2 \pm .70$                               | $-12.25 \pm .98$                             |
| 3.8  | .590   | $11.37 \pm 2.23$                             | $-13.26 \pm 1.36$                            |
| 4.2  | .651   | $12.68 \pm .80$                              | $-15.65 \pm 1.61$                            |
| 4.6  | .712   | $15.23 \pm .60$                              | $-17.6 \pm 1.07$                             |
| 5.0  | .773   | $17.05 \pm .54$                              | $-17.68 \pm 1.52$                            |
| 5.4  | .834   | $20.08 \pm 3.44$                             | $-17.15 \pm 2.62$                            |

Table 3: Data collected for the change in spatial frequency for each image taken at the respective magnetic field for the  $6s7s \ ^3S_1 \ m_j=-1$  to  $6s6p \ ^3P_2 \ m_j=-1$  spin state transition and  $6s7s \ ^3S_1 \ m_j=1$  to  $6s6p \ ^3P_2 \ m_j=1$  spin state transition.

For each image the change in spatial frequency values are made up of radii of the  $R_n$ ,  $R_{n+1}$ , and  $R_{m+j}$ , or  $R_{m-j}$  peaks and then averaged. The averaged data provides the vertical error bars with a 95% confidence the true value of the  $\Delta\nu$  is within that range. See Figure 7. Both the vertical and horizontal error bars also reflect the propagated uncertainty due to measurement in radius and magnetic field respectively. The uncertainty in the slope and intercept of the least squares fit line was calculated according to page 132 in D.C. Baird's book. [13]

## 4.2 Results and Brief Discussion

Figure 7 displays the calculated change in spatial frequency as a function of magnetic field. When fitting the data for both the  $m_j=-1$ , the inner split peak, and  $m_j=1$ , the inner split peak, the fit lines are within the majority

of error bars and suggests the model represents the system reasonably well. However, error bars are fairly large and suggest improvements can be made to the measurements for those values.

The relation  $\frac{\Delta\nu}{\text{MagneticField}}$  is found as  $-23.74 \pm 4.17 \text{ mm}^{-1}\text{T}^{-1}$  with an intercept of  $.83 \pm 2.76 \text{ mm}^{-1}$  for the  $m_j=-1$  transition. Similarly, a linear relationship of  $28.11 \pm 3.09 \text{ mm}^{-1}\text{T}^{-1}$  with an intercept of  $-4.50 \pm 2.05 \text{ mm}^{-1}$  was found for the  $m_j=1$  spin state transition. The accepted values are  $-23.33 \text{ mm}^{-1}\text{T}^{-1}$  for the  $m_j=-1$  transition and  $23.33 \text{ mm}^{-1}\text{T}^{-1}$  for the  $m_j=1$  transition. The linear values differ from the accepted values by  $+2\%$  and  $+20\%$  respectively.

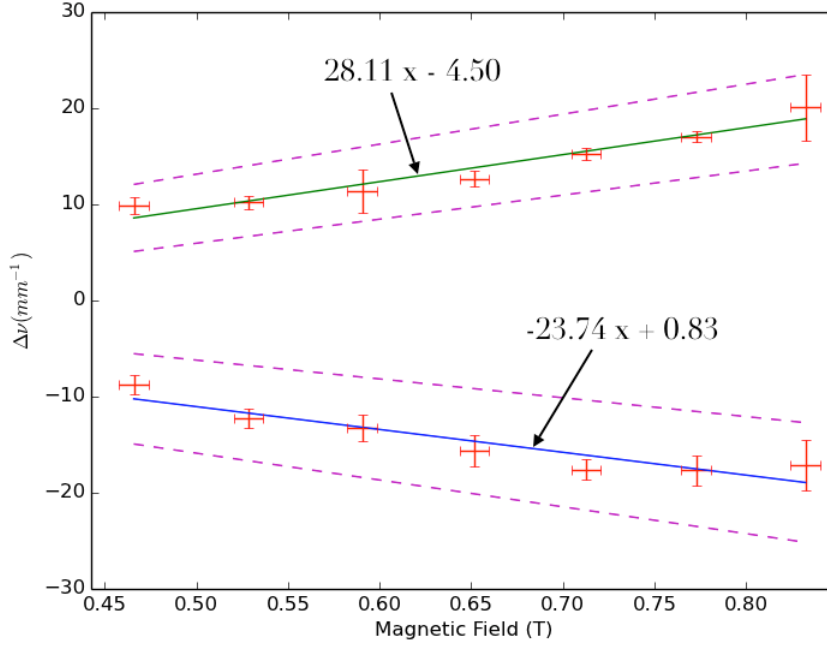


Figure 7: Change in spatial frequency plot as a function of magnetic field.

The magnitudes of  $\Delta\nu$  for  $m_j=1$  and  $m_j=-1$  should equal, according to the theoretical values, however, there is a drastic difference in the observed values. When considering the intensity plot of the 3.4 amps image in Figure 12, there is a noticeable difference in the distance the  $R_{m+j}$  and  $R_{m-j}$  peaks have from the  $R_n$  peak. This is most likely due to off axis imaging from the center of the etalon. The difference suggests future investigations might stand to gain if methods are employed to calculate the different state transitions by accounting for their susceptibility to off axis observations. Perhaps a correction to the calculations is possible based on the skewing of the peaks. One possible method to correct for off axis observations, may be by rotating the cross sections used for the analysis so as to balance the intensity magnitudes at either side of the center and provide a more symmetric cross section.

Also, the method of determining the center of the ring pattern seems admittedly crude. The method also stands to be improved because it consumes the vast majority of the computing time. Although on the order of a few minutes, those minutes are multiplied for each image that is processed. Also, in terms of equipment, the fineness of the Fabry-Perot etalon could be increased to provide sharper peaks and provide more distinct rings for the script to identify.

## 5 Summary and conclusions

The observed values of  $\frac{\Delta\nu}{\text{MagneticField}}$  are  $-23.74\pm 4.17 \text{ mm}^{-1}\text{T}^{-1}$  with an intercept of  $.83\pm 2.76 \text{ mm}^{-1}$  for the  $m_j=-1$  transition, and  $28.11\pm 3.09 \text{ mm}^{-1}\text{T}^{-1}$  with an intercept of  $-4.50\pm 2.05 \text{ mm}^{-1}$  for the  $m_j=1$  spin state transition. These values are generally in agreement with other previous experiments and theoretical values. [2] However, greater agreement can most likely be achieved through improved application of computing methods and an increase in Fabry-Perot etalon fineness to improve peak identification. However, the application of a scripting language has improved the rigor of which the images can be analyzed. Further improvement of this computing method can provide a means to fully automate the analysis for multiple transitions. Such an implementation would include the analysis of the  $^3S_1$  to  $^3P_0$  (violet), and  $^3S_1$  to  $^3P_1$  (blue) state transitions along with the  $^3S_1$  to  $^3P_2$  analysis already provided.

**Acknowledgements:** Thanks to Jason Koeller for beginning this experiment and to Ana Loya for loaning her Canon Rebel T1i camera. Also, a special thanks go to Dr. Sitz for the invaluable advice provided.



## References

- [1] ZEEMAN, P. (1897). The effect of magnetisation on the nature of light emitted by a substance. *Nature*, 55(1424), 347-347. doi:10.1038/055347a0
- [2] *Journal of Physical and Chemical Reference Data* 35, 1519 (2006); doi: 10.1063/1.2204960
- [3] Herzberg, G. (1944). *Atomic spectra and atomic structure*. 2d ed. New York: Dover. p. 202
- [4] Melissinos, Adrian C. 1929- (Adrian Constantin), and Napolitano, J. (2003). *Experiments in modern physics*. San Diego: Academic Press.
- [5] [http : //www.hep.wisc.edu/ prepost/407/zeeman/zeeman.pdf](http://www.hep.wisc.edu/prepost/407/zeeman/zeeman.pdf)
- [6] Hariharan, P. (2010). *Basics of Interferometry*. Retrieved from <http://www.ebib.com>
- [7] Griffiths, D. J. (2005). *Introduction to quantum mechanics* (2nd ed.). Upper Saddle River, NJ: Pearson Prentice Hall.
- [8] [https : //github.com/Lothilius/thezeemancometh/](https://github.com/Lothilius/thezeemancometh/)
- [9] [http : //scikit - image.org/](http://scikit-image.org/)
- [10] [http : //mxp.physics.umn.edu/s11/Projects/S11OpticalPumping/theory2.htm](http://mxp.physics.umn.edu/s11/Projects/S11OpticalPumping/theory2.htm)
- [11] [http : //docs.scipy.org/doc/numpy/reference/](http://docs.scipy.org/doc/numpy/reference/)
- [12] *Canny, J., AComputationalApproachToEdgeDetection, IEEETrans.PatternAnalysisandMach* 679 – 714, 1986
- [13] Baird, D. C. (1995). *Experimentation: an introduction to measurement theory and experiment design*. 3rd ed. Englewood Cliffs, N.J.: Prentice Hall.

# A Mercury Transition Structure

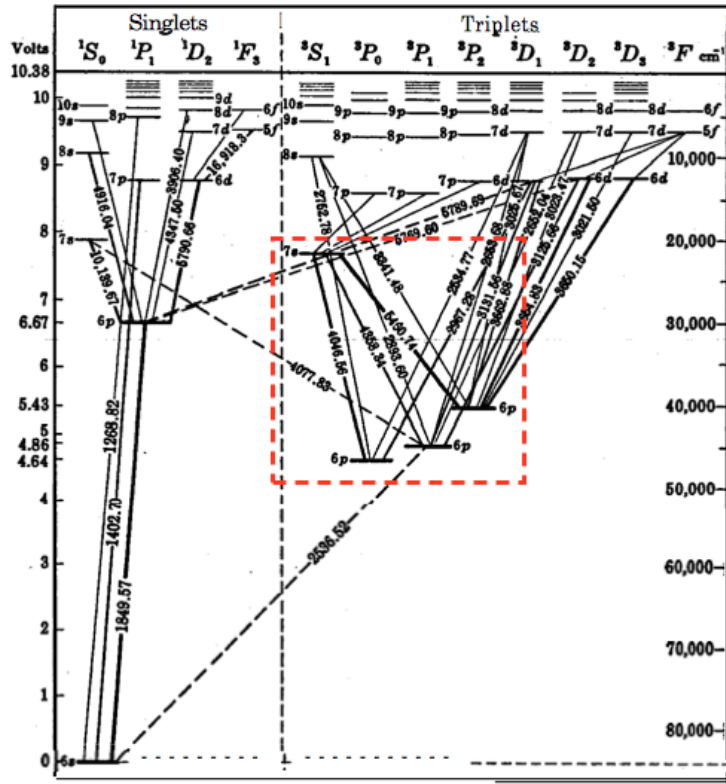


Fig. 75. Energy Level Diagram of Hg I [Grotrian (8)]. The wave lengths of the more intense Hg lines are given (cf. Fig. 6, p. 6). The symbols  $6p$ , etc., written near each level, indicate the true principal quantum number and the  $l$  value of the emission electron.

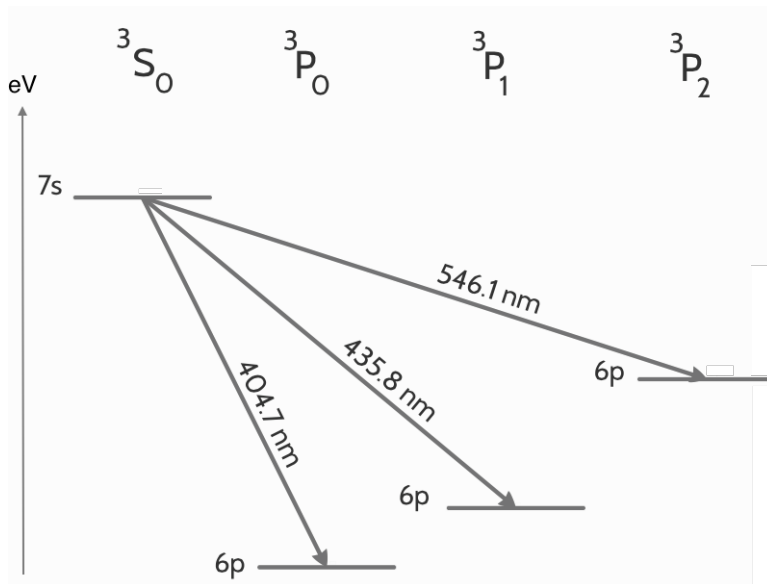


Figure 8: The image at the top of the page is of the atomic structure of the Hg atom taken from Herzberg, G. (1944). Atomic spectra and atomic structure. 2d ed. New York: Dover. p. 202. The lower image is a larger display of the red rectangle in the image at the top. The displayed transitions in the lower image are with no magnetic field.

## B Zeeman Calculation

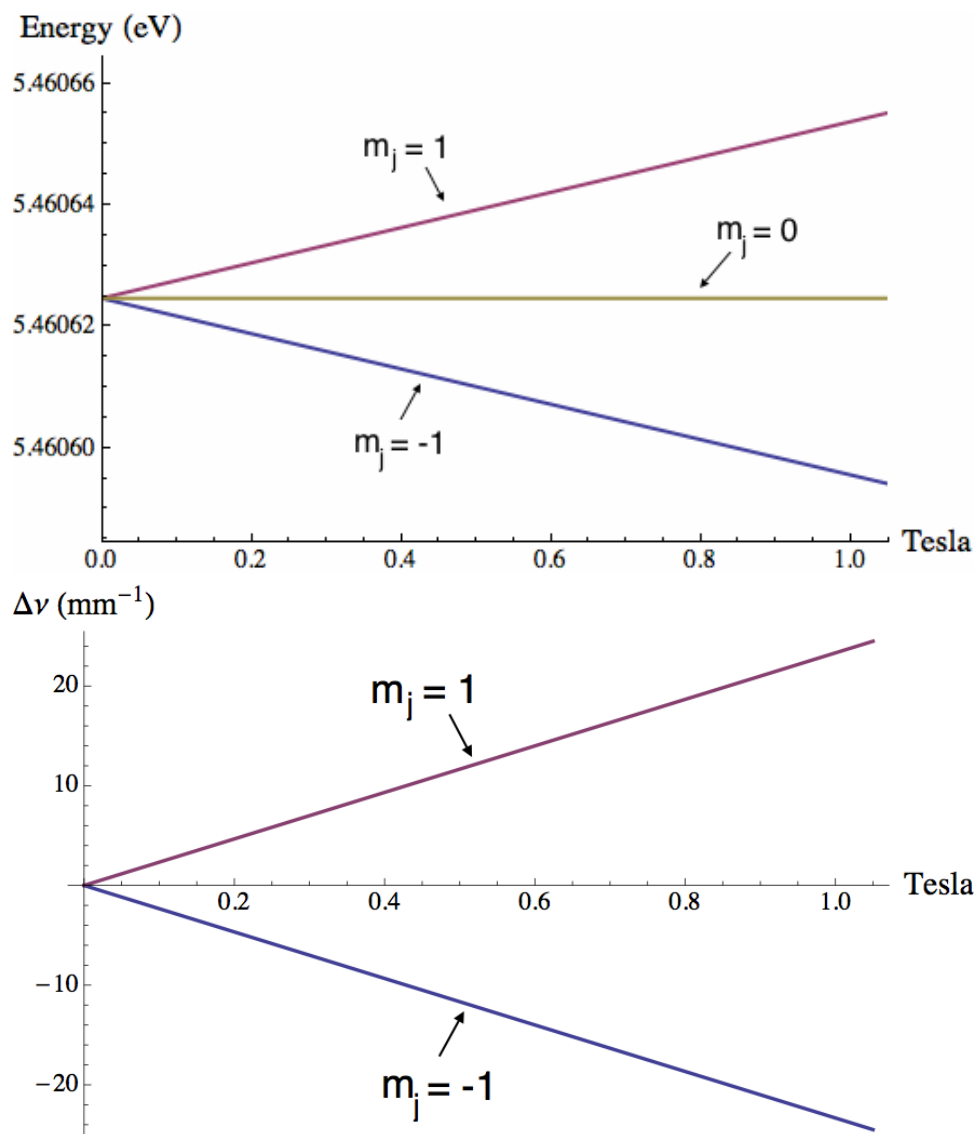


Figure 9: The top plot displays the theoretical values for Energy of the transition of the  $6s7s\ ^3S_1$  split states to the split states of  $6s6p\ ^3P_2$ ,  $m_j = \pm 1$ , and 0. The bottom plot depicts the theoretical change in spatial frequency for the  $m_j = \pm 1$  transitions.

### C Fringe Images

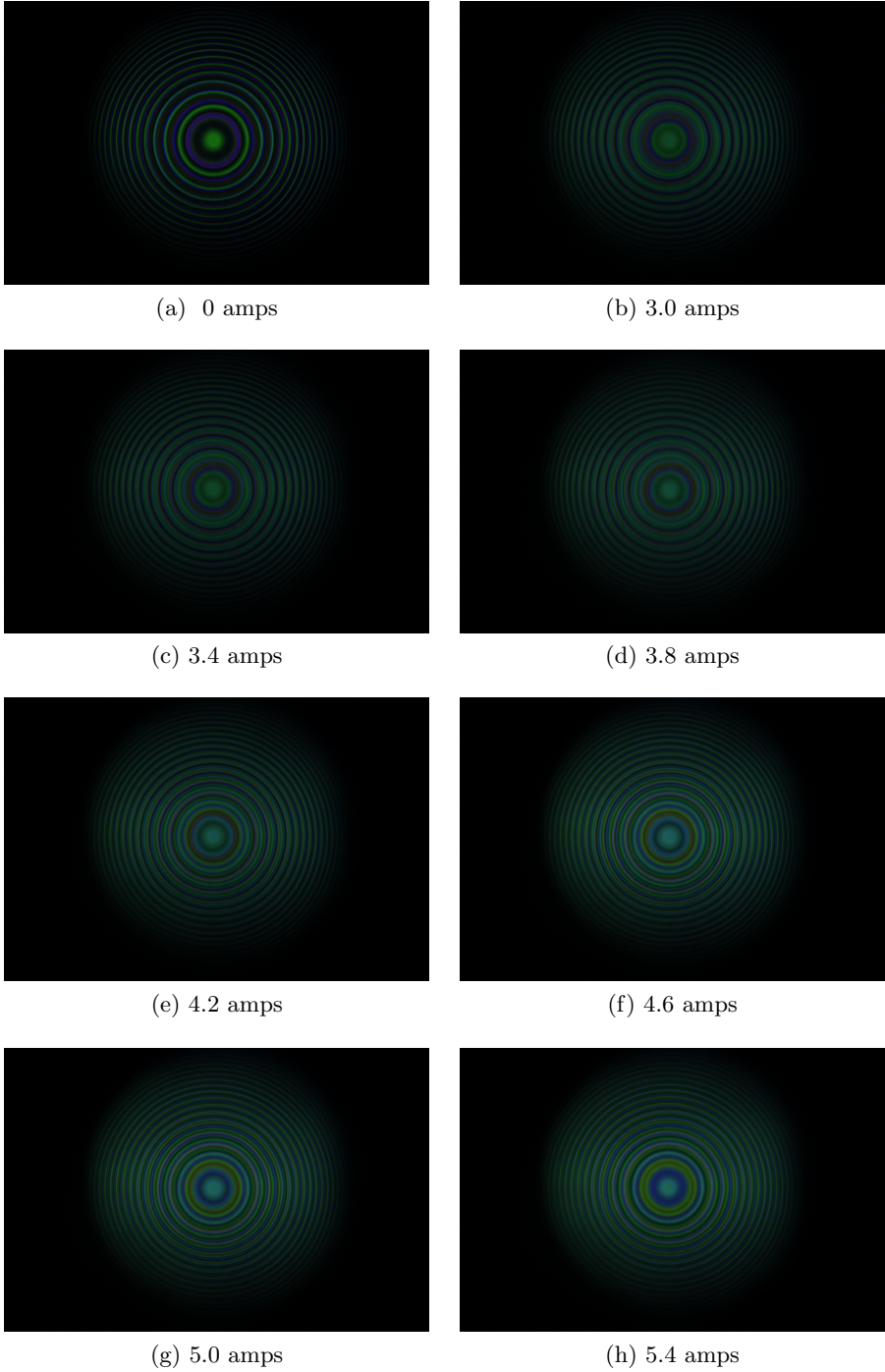


Figure 10: Images of the observed fringes.

## D Perturbation Theory

The structure of the  $\text{Hg}^{198}$  is altered when a uniform magnetic field  $B$  is present. In order to treat these conditions it is necessary to treat the issue with Perturbation Theory. Therefore the correct Hamiltonian is made of the typical Hamiltonian, spin orbital correction, and a magnetic Field term. [7]

$$\bar{H} = \bar{H}_0 + \bar{H}_{LS} + \bar{H}_B \quad (3)$$

For an electron the correct quantum numbers are made of coupling the angular momentum  $\vec{L}$  and the orbital momentum  $\vec{S}$  in to a new angular vector  $\vec{J}$ .

$$\vec{L} + \vec{S} = \vec{J} \quad (4)$$

This coupling breaks degeneracies present when taking  $\vec{L}$  and  $\vec{S}$  independently.

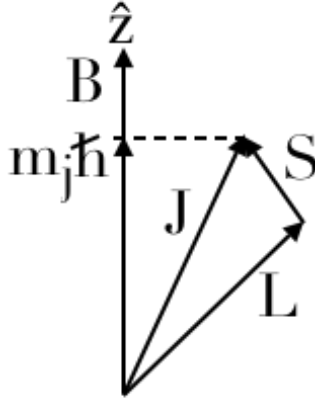


Figure 11:  $\vec{S}$  and  $\vec{L}$  coupling diagram to produce the coupled  $\vec{J}$  vector.

$$\Delta E = g_F \mu_B m_j B \quad (5)$$

Here  $\Delta E$  is the change in Energy from the original un-split state;  $g_F$  is the combined g-factor that results from the vector combination discussed for equation 4;  $\mu_B$  is the Bohr magneton;  $m_j$  is the  $\hat{Z}$  projection of the spin-orbit coupled vector  $\vec{J}$ ;  $B$  is the magnetic field. [7] The theoretical values are provided in Appendix B in Figure 9. It is this change in photo emission wavelength we are investigating by using a variable magnetic field.

## E Code Snippets

### E.1 Filtering

Image files can be converted to "matrix" values in python using the "data.load([full path and name])" function. Assigning the output of this function to a variable provides access to the RGB intensity values for each pixel of the image. So, for any pixel in the image a list of three intensity values will be given; [Red, Green, Blue]. By removing the values of the red and blue intensities the image is left with only the green values and thus acts as a filter. The following snippet of code contains a brute force method of filtering the color of an image, "image\_rgb".

```
1 image_rgb = data.load(full_path)
2 colorow = np.array([[0, 1, 0]] * len(image_rgb[0]))
3 image_stripped = np.array([colorow] * len(image_rgb))
4 image_stripped = image_stripped * image_rgb
```

In line one the code imports an image to the variable name "image\_rgb" then in lines 2 and 3 a numpy array of the same size as the "image\_rgb" matrix is created, however, the red and blue values are all 0 but the green values are all 1. So that the expanded print out of the variable "colorow" for a 2 x 3 "image\_rgb" will be as follows:

```
[0 1 0], [0 1 0], [0 1 0]
[0 1 0], [0 1 0], [0 1 0]
```

Because the code creates numpy arrays we are able to use the multiplication function of the two matrices on line 4 so that if we have "image\_rgb" as follows:

```
[16 22 36], [15 25 35], [15 30 35]
[17 47 23], [15 45 19], [13 43 17]
```

The multiplication of "image\_rgb" and "image\_stripped" will have a print out that will only have the green components to each pixel, as in the following:

```
[0 22 0], [0 25 0], [0 30 0]
[0 47 0], [0 45 0], [0 43 0]
```

## E.2 Peak Radii

In Figure 12 the images show a comparison of the zero amps image with the 3.4 amps image. As can be seen in the zero amps image the peak intensities are much more clear than that of the 3.4 amps. This clarity in peaks is the primary the reason to use the zero amps image as a way to establish a range for each peak detection. Because of the sharp peaks present in the zero amps image, the Canny function has a greater chance at detecting the edges of the peaks and provide two pieces of useful information. The first is a clear representation of the fringe pattern, which can be used to determine the center of the fringes, and second, it establishes boundaries for which to look for intensity peak locations. The center determination is discussed in Appendix E.3.

```
1 import skimage as ski
2 image_stripped = rgb2gray(image_stripped)
3 image_proc = ski.filter.canny(image_stripped, sigma=4,
    low_threshold=0, high_threshold=7)
```

In python the Skimage package must be imported before use of Canny filter. Line 1 converts the filtered image to a grey scale image. Line 3 provides the use of the Canny filter on the grey scale image "image\_stripped". Beside the variable name of the image three parameters are passed to the Canny filter; sigma, low and high hysteresis thresholds. The Canny filter is made of two sub-filters, first performing Gaussian smoothing, then Sobel edge detection. [12] The sigma parameter provides a blurring parameter in terms of standard deviations of the pixel. The Gaussian filter serves to reduce noise in the image and there by reducing the possibility of false positive edge detection. The Sobel edge detection provides the actual detection of the edges of the fringes by calculating a gradient and its direction for each pixel. Once the Sobel edge detection is complete the Canny filter uses the low and high hysteresis thresholds as a guideline to label each pixel as an edge. The resulting print out of the "image\_proc" variable provides an array of the same dimensions as the initial image, however, in place of the intensity values, the values of each pixel will be a boolean providing wether the pixel in the original image is an edge or not. Please see Figure 13 and example print out of the zero Tesla image.

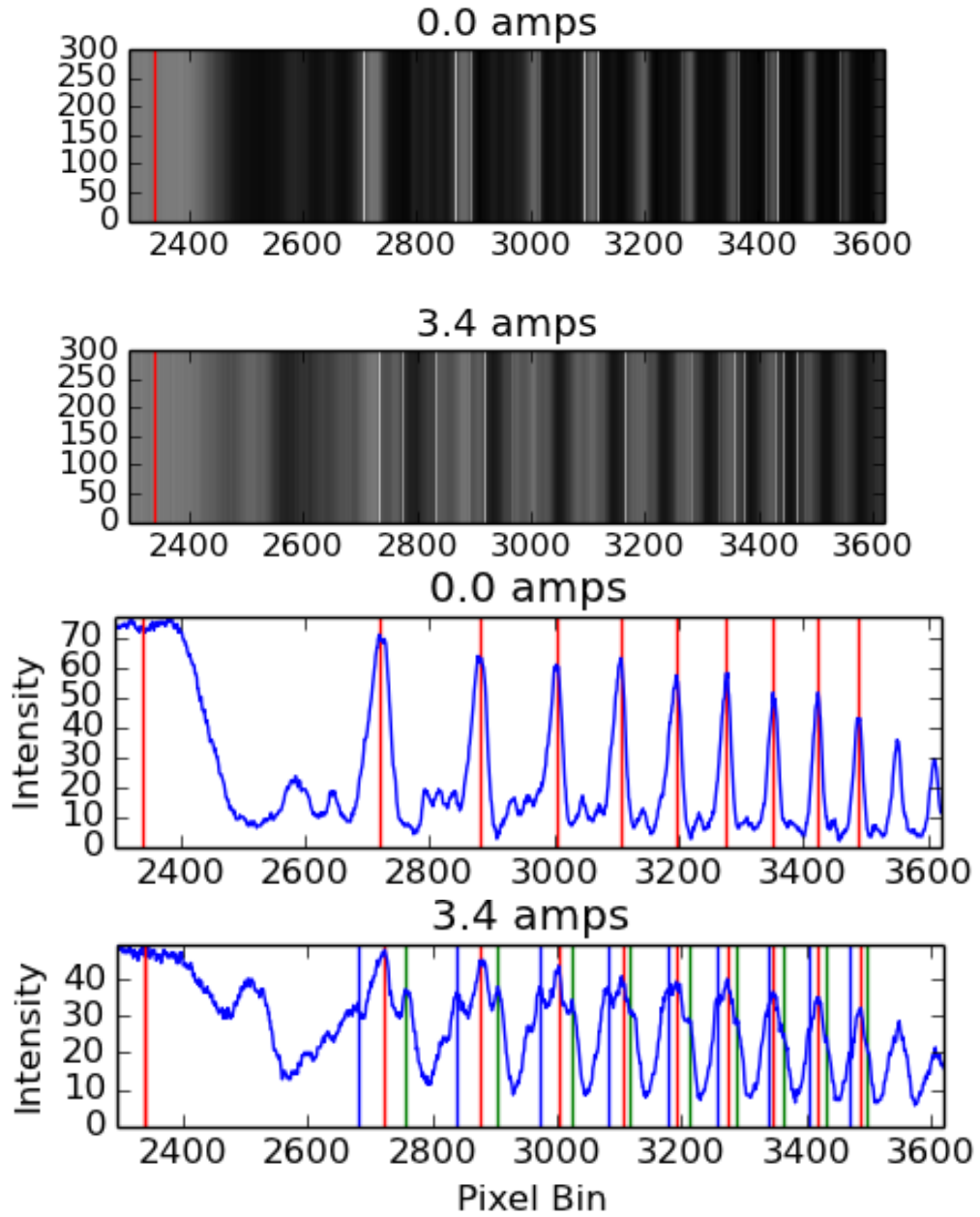


Figure 12: The top images display the right half of the center cross sections duplicated enough to show the intensity pattern. White lines are the result of the Canny edge detection function. The bottom two plots display the intensities for the same sections. Green lines are the the intensity peaks of the  $m_j=-1$  transition, and blue lines are for the  $m_j=1$  transition. The red line at the left of all the images is the center of the rings along the x axis and each following red line are that of the  $m_j=0$  transition.



### E.3 Determining the Center

Determining the center of the fringe pattern is done through the use of the `hough_circle` function in the Scikit-image processing package. The function uses the output of the Canny edge detection filter to trace out the edges of the first set of rings.

```
1 import skimage as ski
2 image_proc = ski.filter.canny(image_stripped, sigma=4,
    low_threshold=0, high_threshold=7)
3 hough_radii = np.arange(350, 425, 5)
4 hough_res = ski.hough_circle(image_proc, hough_radii)
...
5 for radius, h in zip(hough_radii, hough_res):
6     # For each radius, extract two circles
7     peaks = peak_local_max(h, num_peaks=2)
8     centers.extend(peaks)
9     accums.extend(h[peaks[:, 0], peaks[:, 1]])
10    radii.extend([radius, radius])
...
11 # Draw the most prominent 15 circles
12 for idx in np.argsort(accums)[::-1][:15]:
14     center_x, center_y = centers[idx]
15     radius = radii[idx]
16     center_array.append([center_x, center_y])
17     cx, cy = circle_perimeter(center_y, center_x, radius)
18     image[cy, cx] = (220, 0, 0)
```

The first section of the code uses the "hough\_circle" function to detect the potential circle components in the image of radius between 350 and 435. The second section of the code uses the "peak\_local\_max" to determine the location of the circles. The third section of the code is used for re-packaging the circle information to an image array which can be print out as an image such as in Figure 13. Also, in section 3 the centers of the detected circles is gathered for later determining the average center point. Because determining the center of the fringe pattern is time intensive, a method to better narrow the radius range on line 3 could greatly improve efficiency. The radius range in line 3 was determined by manual estimation for the current implementation.

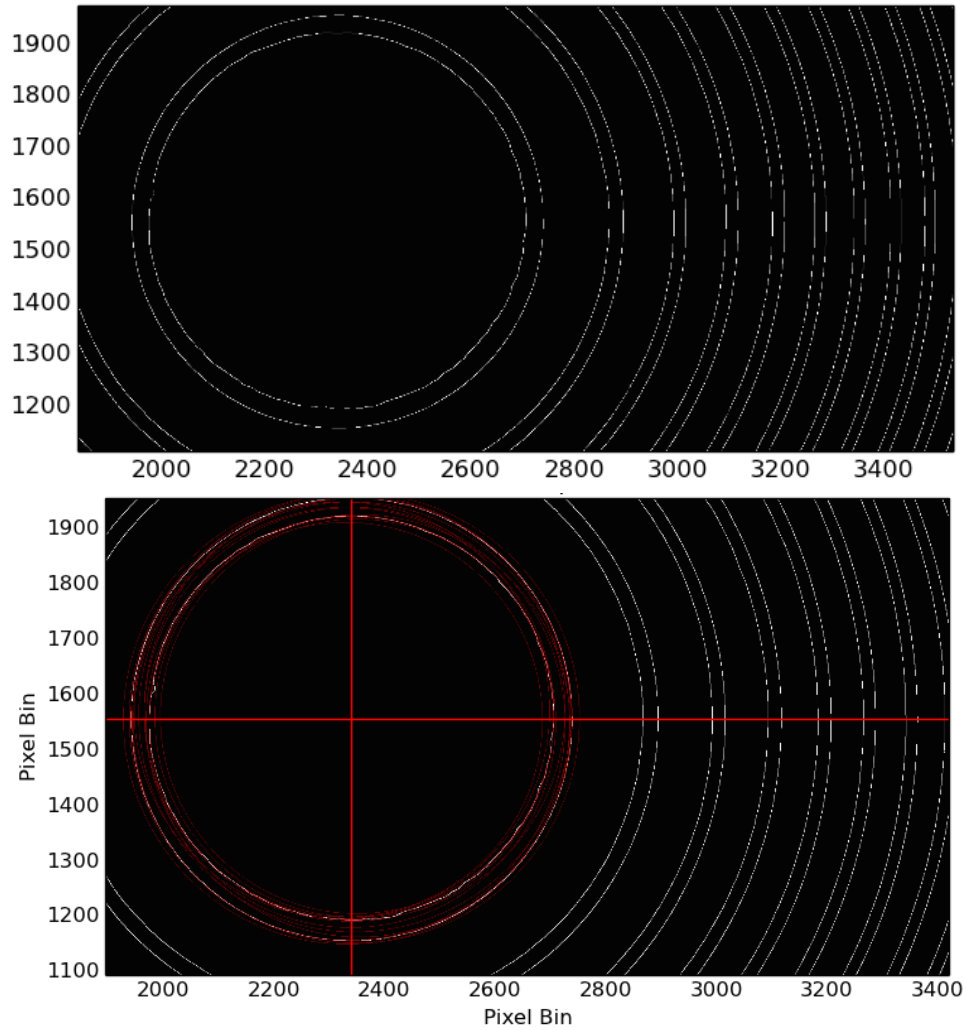


Figure 13: The top image is section of the Canny filter image. The white lines are the detected edges of one pixel in thickness. Because of the the narrow thickness not all pixels of the edges are printable on the image, however, if we were to zoom in on the image we can verify the detected edges are continues. Similarly the bottom image does not display all pixels of the Canny detected edges or of the detected circles in red.